A self-driven photodetector based on a SnS_2/WS_2 van der Waals heterojunction with an Al_2O_3 capping layer

Hsiang-Chun Wang(王祥骏)[1], Yuheng Lin(林钰恒)[1], Xiao Liu(刘潇)[1], Xuanhua Deng(邓煊华)[1], Jianwei Ben(贲建伟)[1], Wenjie Yu(俞文杰)[2], Deliang Zhu(朱德亮)[1], and Xinke Liu(刘新科)[1,†]

[1] *College of Materials Science and Engineering, Institute of Microelectronics (IME), Guangdong Research Center for Interfacial Engineering of Functional Materials, Shenzhen University, Shenzhen* 518060, *China*

[2] *State Key Laboratory of Functional Materials for Informatics, Shanghai Institute of Microsystem and Information Technology, Chinese Academy of Sciences, Shanghai* 200050, *China*

(Received 17 January 2022; revised manuscript received 26 March 2022; accepted manuscript online 7 May 2022)

Photodetectors based on two-dimensional (2D) materials have attracted considerable attention because of their unique properties. To further improve the performance of self-driven photodetectors based on van der Waals heterojunctions, a conductive band minimum (CBM) matched self-driven SnS_2/WS_2 van der Waals heterojunction photodetector based on a SiO_2/Si substrate has been designed. The device exhibits a positive current at zero voltage under 365 nm laser illumination. This is attributed to the built-in electric field at the interface of the SnS_2 and WS_2 layer, which will separate and transport the photogenerated carriers, even at zero bias voltage. In addition, the Al_2O_3 layer is covered by the surface of the SnS_2/WS_2 photodetector to further improve the performance, because the Al_2O_3 layer will introduce tensile stress on the surface of the 2D materials leading to a higher electron concentration and smaller effective mass of electrons in the films. This work provides an idea for the research of self-driven photodetectors based on a van der Waals heterogeneous junction.

Keywords: SnS_2/WS_2 heterogeneous junction, Al_2O_3 layer, self-driven, photodetector

PACS: 85.60.Bt, 85.60.Gz, 68.47.Fg, 73.40.Lq **DOI:** 10.1088/1674-1056/ac6dbd

1. Introduction

Since the discovery of graphene, two-dimensional (2D) materials have been considered as promising candidates to replace silicon-based optoelectronic devices because of their high flexibility, excellent carrier transmission and designable interface characteristics.[1–5] However, graphene is limited in many fields due to its zero bandgap. As substitutes for graphene, 2D transition metal dichalcogenides (TMDCs) are two-dimensional semiconductor materials that have been widely studied.[6–10] The transition metal sulfide molecular formula is MX_2 (M = W, Sn, Mo, etc., and X = S, Te or Se), and the molecular structure is the sandwich-like structure of XMX. Compared with graphene, TMDCs have an adjustable bandgap of 1 eV–3 eV, which makes them suitable for the preparation of photodetectors, solar cells, FETs and gas sensors, etc.[11–22] In particular, TMDCs have the potential to achieve high-efficiency photodetectors due to the high absorption coefficients in the ultraviolet and visible regions. SnS_2 has an indirect bandgap of $\sim$ 2.3 eV, which is stable with the change of thickness.[23,24] It has been reported that the carrier mobility of a SnS_2based ultra-thin transistor was about 50 $cm^2/(V{\cdot}s)$ and a high onoff current ratio of 10^6 has been achieved, thus making SnS_2 a favorable material for the fabrication of photodetectors.[25] It has been reported that an ultraviolet (UV) to near-infrared (NIR) photodetector based on a SnS_2 nanosheet and microsphere film have been achieved, showing remarkable performance.[26,27] Tungsten disulfide (WS_2), one of the TMDCs, is a potential candidate for various electrical and optical applications due to its large and distinctive tunable bandgap (1.3 eV–2.1 eV).[28] When the thickness of WS_2 decreases to a single layer, the band structure of WS_2 will transform from indirect to direct.[29] The carrier mobility of 2D WS_2 has been reported as high as 232 $cm^2/(V{\cdot}s)$. The band structure of 2D WS_2 shows relatively large valence band splitting compared with other 2D TMDCs materials, which makes the Hall effect easier to observe.[30] In addition, WS_2 can be used as a lubricant in a wide range of operating temperatures, which is attributed to its high thermal stability.[31] However, SnS_2 based detectors have a low operating speed, and the existence of surface defects is one of the causal factors.[23,32,33] To solve the problem, the surface passivation method has been adopted. It has been reported that the surface of 2D SnS_2 material can be passivated to reduce surface defects, decrease response time and improve the responsivity.[12] Meanwhile, high-sensitivity photodetectors based on WS_2 can also be realized through interface passivation.[34]

The development of energy saving and environmental protection devices is the general trend. Under this background, one of the main challenges for the next generation of photodetectors is to reduce the overall power consumption. As a result, self-driven photodetectors are increasingly attracting attention.[35–37] Compared to conventional photodetectors, self-driven photodetectors exhibit ultra-low

†Corresponding author. E-mail: xkliu@szu.edu.cn

© 2023 Chinese Physical Society and IOP Publishing Ltd

dark current and noise, resulting in a very high signal/noise ratio. From this viewpoint, self-driven photodetectors are confirmed to be the best candidates for the next generation of photodetectors.[37,38,43] Combining the advantages of 2D materials, self-driven photodetectors based on 2D material heterogeneous junctions have been reported.[44–46] For example, a photodetector based on a monolayer MoS_2/WS_2 heterojunction structure has shown good performance with responsivity of 4.36 mA/W and detectivity (D^*) of 4.36×10^{13} Jones under 532 nm wavelength.[45] It has been reported that visible phototransistors based on nanolayered heterostructures of SnS/SnS_2 and $SnSe_2/SnS_2$ show very high photoresponsivity of 3567 A/W and 1793 A/W, respectively.[46] However, heterostructure photodetectors with excellent self-driven performance and good rectification effectively prepared by other 2D materials urgently need research. Therefore, SnS_2 has a suitable bandgap and better optical absorption characteristics, but the higher photosynthetic electron–hole composite leads to a slow response time in the device, limiting its application in the field of photodetectors. WS_2 demonstrates excellent optical response performance, and also has higher electron mobility due to its smaller electron effective mass. In this work, a SnS_2/WS_2 van der Waals heterojunction photodetector has been fabricated on a SiO_2/Si substrate. As reported, depositing a surface passivation layer reduces the surface defects of the materials and introduces tensile stress to modify the intrinsic properties.[12,34] Furthermore, the device designed with 3-nm-thick Al_2O_3 as a passivation layer and stress liner on the surface demonstrates better self-power and photoelectric detection performance than the initial device. The photodetector shows good detection, and the photoresponsivity of the device has been increased four times by covering the Al_2O_3 layer. Under illumination of 365 nm and 0 V bias voltage, the SnS_2/WS_2 photodetector with the Al_2O_3 modified layer exhibits high photoresponsivity of 4.57 A/W and detectivity of 8.07×10^{10} Jones (input power of 11.10 nW), which demonstrates relatively good self-power and high photo-responsivity performance. These results therefore provide an idea for the next generation of photodetectors.

2. Experimental details

Firstly, WS_2 crystals were mechanically peeled and transformed by adhesive tape onto the insulating Si wafer (with 300 nm SiO_2 on the Si surface). The WS_2 nanosheets with a thickness of about 10 nm were found using an optical microscope, and the specific location was marked. Then, the SnS_2 was transferred to the PDMS film via the same mechanical stripping process. Under the optical microscope, the target SnS_2 was transferred to the target WS_2 to construct the SnS_2/WS_2 heterojunction. Then, electron beam exposure (EBL, Raith EBPG 5150, Pioneer 2) was used to write the electrode pattern, and a thermal evaporator (ASB-EPI-C6) was used to deposit the titanium/gold (5 nm/50 nm) electrode to prepare the devices. Finally, a 3-nm-thick Al_2O_3 passivation layer (stress liner) was grown on the surface of the SnS_2/WS_2 heterogeneous structure at 300 °C by an atomic layer deposition (ALD) process using trimethylaluminum (TMA1) as the precursor.

3. Results and discussion

The self-driven photodetector is fabricated based on the SnS_2/WS_2 heterogeneous junction in this work. A schematic diagram of the heterojunction photodetector is shown in Fig. 1(a) and the preparation procedure is introduced in Section 2. The SnS_2/WS_2 heterogeneous junction was illustrated by optical microscopy, as presented in Fig. 1(b). Atomic force microscopy (AFM) is used to characterize the morphology and structure, figure 1(c) is the height profile across the edge of the heterojunction region and the inset is the AFM image of the location. Confirmed by AFM, the thicknesses of the SnS_2 and WS_2 layers are about 60 nm and 10 nm, respectively. The Raman spectra of SnS_2, WS_2, and the heterostructure regions are plotted in Fig. 1(d). The Raman spectra were applied to confirm whether the WS_2 and SnS_2 layers were effectively transferred by comparing the spectra before and after transfer. The spectrum of isolated SnS_2 (red) shows one dominant peak at 314.1 cm^{-1} attributed to the out-of-plane A_{1g} mode. The Raman spectra of individual WS_2 (blue) have two typical peaks located at 350.2 cm^{-1} and 420.8 cm^{-1} that can be attributed to the in-plane E^1_{2g} phonon mode and the out-of-plane A_{1g} mode, respectively. The Raman peaks of the heterostructure region (black) exhibit the characteristic vibration modes of both SnS_2 and WS_2; no obvious peak shift was observed in the heterojunction area, indicating that the high quality of the two materials remains in the junction region after transfer. From the spectrum, it can be concluded that the two-dimensional layered materials were transferred and almost no defects were induced during the transfer process.

By considering the band structure and the thickness of SnS_2 and WS_2,[29,47] an energy band alignment diagram of the SnS_2/WS_2 heterogeneous junction is presented in Figs. 2(a) and 2(b). The electron affinities of WS_2 and SnS_2 are nearly matched, which makes the SnS_2/WS_2 heterogeneous junction suitable for design and fabrication as photodetectors. The photogenerated carriers can be well separated in the depletion region due to the existence of ΔE_c, and the electrons can be smoothly transported because there is almost no electronic barrier in the conductive band. As a result, the SnS_2/WS_2-based heterogeneous junction presents self-driven performance. In our previous reports, the Al_2O_3 layer can be used to improve the performance of photodetectors, which

is also applicable in this work.[12,48,49] Figure 2(c) exhibits the comparative Raman spectra of the SnS_2/WS_2 heterogeneous junction region and the heterostructure with the Al_2O_3 capping layer after the ALD process. In contrast with the control SnS_2/WS_2 heterojunction and the heterostructure deposited with the Al_2O_3 capping layer, the Raman intensity and the shift of each characteristic phonon mode peak of the two samples are the same. Obviously, the SnS_2/WS_2 heterostructure modified by the Al_2O_3 layer has shown red-shifts of the Raman characteristic vibration modes peak, attributed to the strain effect introduced by the tensile stress liner as well as the changes in bond lengths and angles in the lattice structure. It is proved that the existence of Al_2O_3 brought neither a compositional evolution nor a microstructural change in the heterostructure.

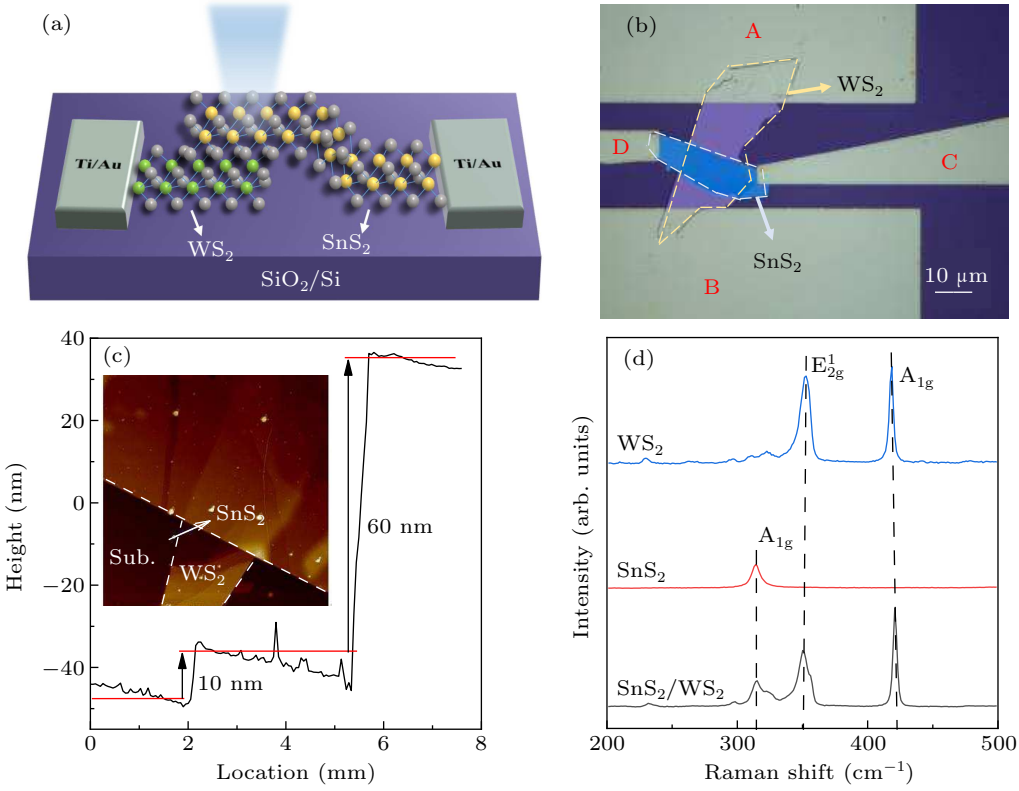


Fig. 1. (a) A schematic diagram of the self-driven SnS_2/WS_2 UV photodetector. (b) An optical microscopy photograph of the device. (c) The thickness of the WS_2 and SnS_2 layers; the inset shows the morphologies of the heterojunction region measured by AFM. (d) The Raman spectra of WS_2 (blue line), SnS_2 (red line) and the SnS_2/WS_2 heterojunction (black line).

We then characterized the performance of the SnS_2/WS_2 heterogeneous junction as a photodetector and the improvement of the photocurrent by the deposited Al_2O_3 capping layer. Firstly, the heterojunction is constructed by dry transfer. Then, EBL technology is used to write four-electrode patterns, as shown in Fig. 1(b). The A and B electrodes are placed on both ends of the SnS_2 sheets, and the C and D electrodes are placed on both ends of the WS_2 sheets. Finally, the electrical properties are tested before and after the deposition of the Al_2O_3 layer. Figures 2(d)–2(f) show the *I*–*V* curves of the photodetectors based on SnS_2 (C–D), WS_2 (A–B), and the SnS_2/WS_2 heterogeneous junction (A–C) with/without an Al_2O_3 layer that were exposed to the light of laser wavelengths (365 nm) and in the dark, respectively. The *I*–*V* curves of the WS_2 and SnS_2 under 365 nm light are presented in Figs. 2(d) and 2(e); the dependence of the current and voltage shows a linear relationship, which indicates the ohmic contact is formed between the layered semiconductor and metal electrodes (Ti $\sim$ 5 nm, Au $\sim$ 50 nm). It is observed that the photocurrent significantly improves after depositing the Al_2O_3 modified layer. As reported in our previous reports,[12,48,49] the enlarged photocurrent can be attributed to the Al_2O_3 layer and will introduce tensile stress in the surface of layered TMDCs, which causes a higher electron concentration and smaller effective mass of the carriers. From the *I*–*V* rectification characteristics of the SnS_2/WS_2 heterogeneous junction indicated in Fig. 2(f), it can be observed that the heterojunction device has rectification characteristics but, due to the matching of the conduction band minimum, the reverse current is large and the rectification ratio is low. For the device with Al_2O_3 layers, the rectification effect is insignificant and almost eliminated under the dark state, which is attributed to the lowering of the potential barrier difference in the heterojunction due to the introduction of strain. However, the pho-

tocurrent with the Al_2O_3 modified layer is improved compared to the control under 365 nm incident light at 0 V bias voltage. Moreover, as shown in Fig. 2(f), the photodetector based on the WS_2/SnS_2 heterogeneous junction shows a very low dark current of about 0.01 nA and remains at a low level of 10^{-11} A, indicating the low-noise features of this device. Meanwhile, the photocurrent of the device reaches a level of 10^{-8} A under 365 nm light illumination at zero voltage, which is hundreds of times higher than the dark state current. The device shows an obvious rectification effect and excellent self-driving performance. This is attributed to the built-in electric field at the interface of the WS_2 and SnS_2 layer, where the photogenerated carriers will separate and transport, even at zero bias voltage. Although this inhibits the recombination of the electron–hole pairs, it will extend the lifetime of the carriers, resulting in an improvement in photoconductivity gain and responsivity. And the device has good rectification characteristics due to the existence of the built-in electric field, which inhibits the diffusion of electrons, reducing the dark current and noise power. It was further proved that the SnS_2/WS_2 heterojunction is excellent for use as a self-driven photodetector. Therefore, the photocurrent of the heterojunction device with the Al_2O_3 capping layer has been greatly improved under 365 nm light illumination at zero voltage. However, the tensile stress from the Al_2O_3 modified layer also leads to an increased dark current ($\sim$ 0.05 nA at 0 V) due to a reduction in forbidden bandwidth and barrier height. As shown in Figs. 2(d)–2(f), it can be proved that the Al_2O_3 modified WS_2 layer, SnS_2 layer and SnS_2/WS_2 heterogeneous junction all show higher a photocurrent than those without the Al_2O_3 capping layer.

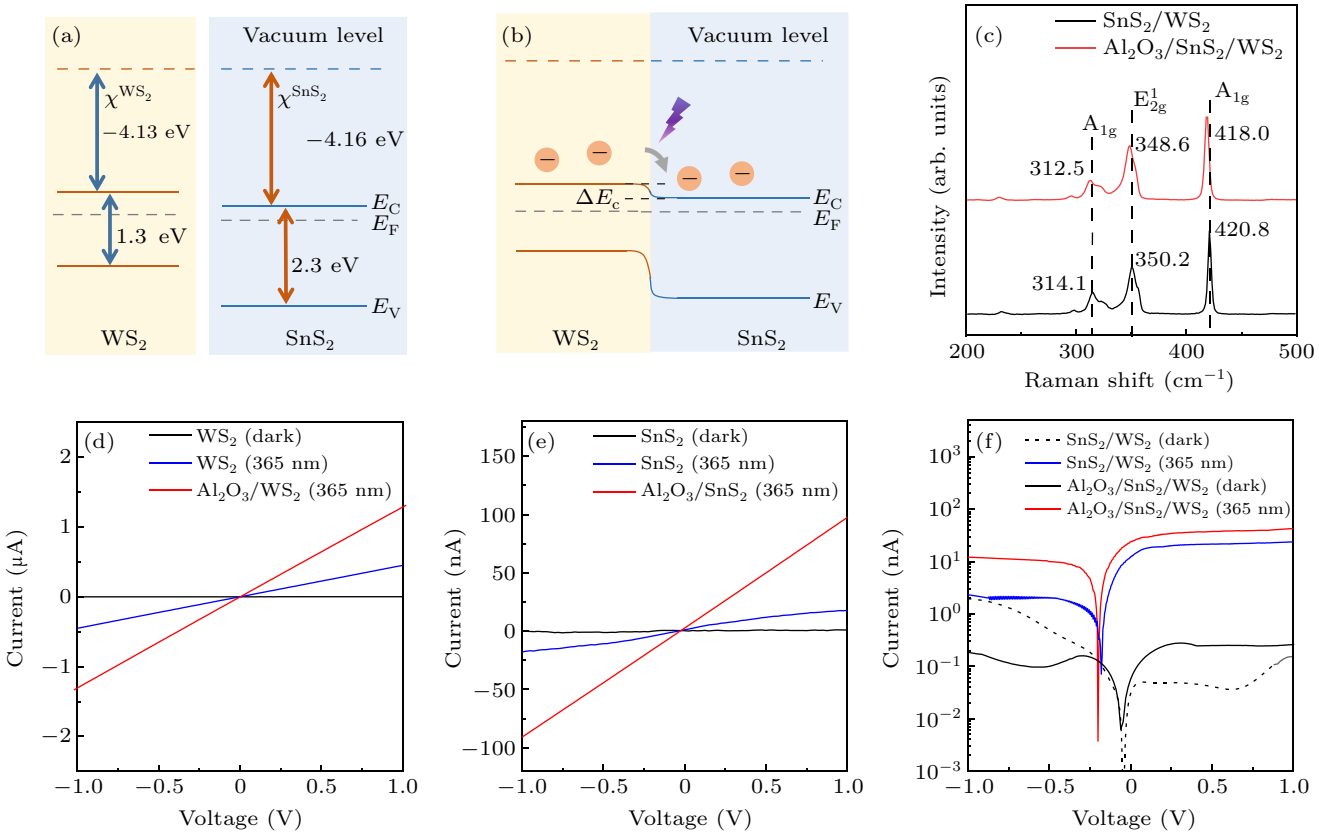


Fig. 2. (a)–(b) The energy band alignment diagram of the SnS_2/WS_2 heterogeneous junction. (c) The Raman spectra of the SnS_2/WS_2 heterojunction (black line) and the sample with the Al_2O_3 capping layer (red line). (d)–(f) The *I*–*V* curves of the samples under dark (black lines) and 365 nm light illumination (blue and red lines) (d) for the WS_2 (blue line) and Al_2O_3/WS_2 (red line) samples, (e) for the SnS_2 (blue line) and Al_2O_3/WS_2 (red line) samples and (f) for the SnS_2/WS_2 heterogeneous junction with (red line)/without (blue line) the Al_2O_3 capping layer.

Based on the *I*–*V* characteristics, the essential performance parameters related to the photodetectors are calculated. The photodetector based on the SnS_2/WS_2 heterogeneous junction is hereinafter referred to as the control sample, while the photodetector with the Al_2O_3 modified layer is hereinafter referred to as the Al_2O_3 modified sample. The responsivity (R), normalized detectivity (D^*), the noise equivalent power (NEP) of the photodetectors and external quantum efficiency (EQE) is calculated using the following formula:[50]

$$R = \frac{|I_{\text{light}}| - |I_{\text{dark}}|}{P_{\text{in}}}, \tag{1}$$

$$\text{NEP} = \frac{\sqrt{2qI_{\text{dark}}\Delta f}}{R_{\text{I}}}, \tag{2}$$

$$D^* = \frac{\sqrt{A}}{\text{NEP}}, \tag{3}$$

$$\text{EQE} = R_{\text{I}} \times \frac{1240}{\lambda} \times 100\%, \tag{4}$$

where I_{light} and I_{dark} are the photo-current and dark-current, respectively. Here, P_{in} is the effective power of the incident light, which is calculated by the total input power divided by the active area (A); and R_I means the responsivity at certain incident laser illumination (λ). The parameter Δf is defined as 1 in this work. As we know, the higher value of R, D^*, and EQE, while the NEP should be as low as possible, means better performance of the devices. The time-dependent photocurrent under 365 nm light irradiation with the bias voltage of 0 V was taken for the control sample and the Al_2O_3 modified sample, as presented in Fig. 3(a). The photocurrent of both samples shows an increasing tendency with the higher input light power. The photocurrent and the incident laser power conform to the formula $I_{ph} \propto P_{in}^{\theta}$, where the calculated value of θ is great than 1; thus, the responsivity shows an increasing trend with the light power, as shown in Fig. 3(b). It can be attributed to the fact that the light absorption in the heterogeneous junction region has not reached saturation, which can be attributed to the traps of the surface defect states that have captured a large number of photogenerated carriers. Therefore, the value of the responsivity increases with the increase in incident light power. From the curves presented in Fig. 3(b), it can be concluded that the performance of the Al_2O_3 modified sample was better than the control sample, and the performance of the photodetectors will be better with higher incident laser power. Figure 3(c) shows the relationship between D^* and NEP of heterojunction-based devices with/without the Al_2O_3 capping layer under different illumination power at 0 V bias voltage. It is observed that the device has low NEP, the D^* can reach 3.36×10^{11} Jones and the EQE reaches 15.4 at 0 V bias voltage with 365 nm light radiation (11.10 nW) for the Al_2O_3 modified sample in Figs. 3(c) and 3(d). Therefore, it can be proved that the Al_2O_3 modified WS_2 layer, SnS_2 layer and SnS_2/WS_2 heterogeneous junction can reach more effective optical detection than that without the Al_2O_3 modified layer. The better performance of the Al_2O_3 modified sample is considered to be attributed to the passivation of the 2D materials' surface states and the tensile stress generated from the Al_2O_3 layer.[12,46,47] The passivation of the surface states will enhance the transport of carriers because the surface states will induce charge scattering. Furthermore, as reported in our previous reports,[12,46,47] the Al_2O_3 modified layers induce tensile stress leading to a higher electron concentration and smaller effective mass of electrons in the films. As a result, the conductivity of the layered materials will be increased and further enlarge the photocurrent.

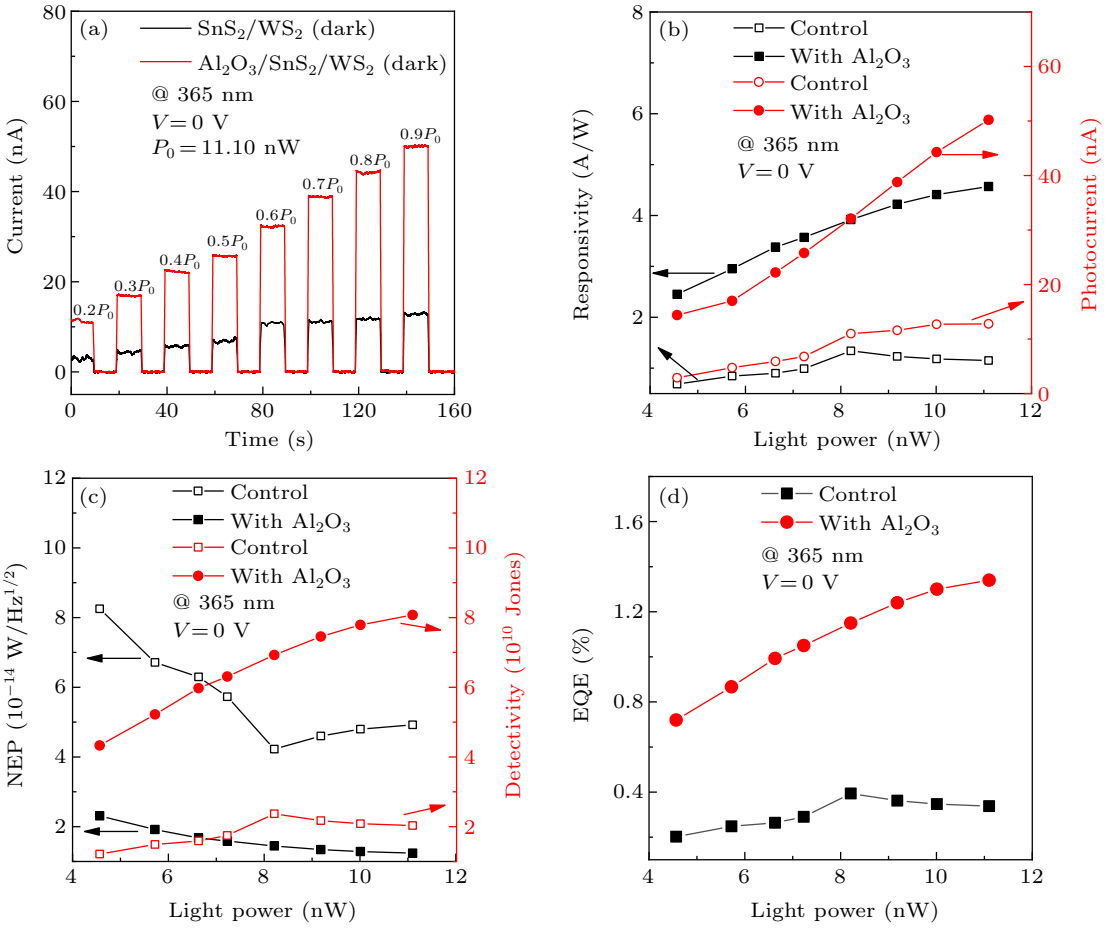


Fig. 3. The self-driven SnS_2/WS_2 van der Waals heterojunction photodetector with an Al_2O_3 layer and the control device under 365 nm illumination at zero bias voltage, for different input light power. (a) The time-dependent current under different incident power of the device with the Al_2O_3 layer (red line) and the control device without the Al_2O_3 layer (black line); (b) the responsivity (black lines) and photocurrent (red lines); (c) the NEP (black lines) and detectivity (red lines); and (d) the EQE of the Al_2O_3 layer device (red line) and the control (black line).

Table 1. Comparison of important performance parameters of the device in this work with other reported performance parameters of photodetectors based on 2D materials.

Devices	R (A/W)	D^* (Jones)	Response time	EQE (%)	Self-driven	Ref.
WS_2/Ge	0.635	4.30×10^{11}	5.3 ms	50.80	Yes	[34]
GaSe/MoS_2	0.670	2.30×10^{11}	155 μs	–	Yes	[44]
MoS_2/WS_2	4.36×10^{-3}	4.36×10^{13}	4 ms	–	Yes	[45]
$MoTe_2$/WTe_2	0.220	3.00×10^{11}	–	–	Yes	[51]
2D-WS_2/GaAs	0.527	1.03×10^{14}	21.8 μs	8	Yes	[52]
GaSe/$MoSe_2$	0.169	6.60×10^{11}	16 ms	39	Yes	[53]
SnS_2/WS_2	1.15	2.37×10^{10}	0.559 s	0.39	Yes	this work
Al_2O_3/SnS_2/WS_2	4.57	8.07×10^{10}	0.302 s	1.34		

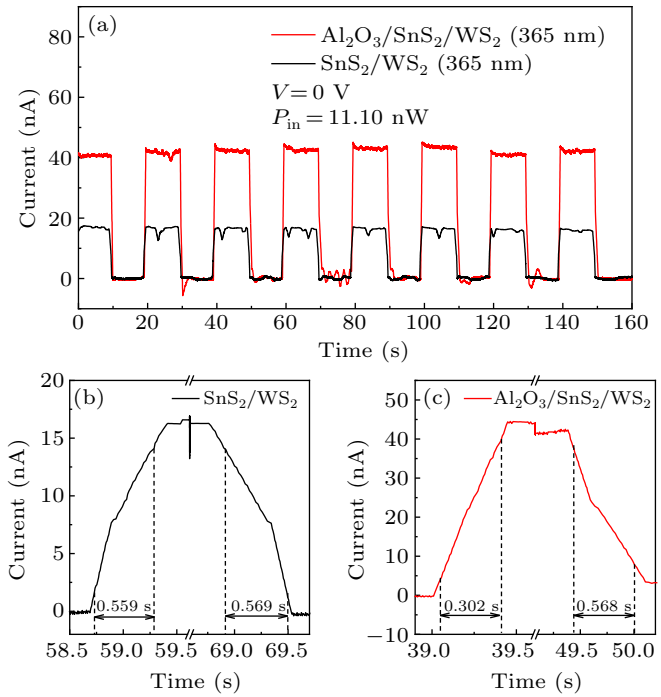


Fig. 4. (a) The time-dependent photocurrent curves of the photodetector with (red line)/without (black line) Al_2O_3 for light power of 11.10 nW. (b)–(c) The single period of the time-dependent photocurrent curves of the control (black line) and with the Al_2O_3 layer (red line) samples with $P_{in} = 11.10$ nW.

The time-dependent photocurrent property is an important indicator of photodetector performance. However, the photocurrent of the Al_2O_3 modified sample shows a better linear relationship with the increase of P_{in} than that of the control sample, which proves that the Al_2O_3 modified sample is more sensitive to the change in input light power. Figure 4(a) exhibits the time-dependent photocurrent curves of the two samples under 365 nm light at the bias voltage of 0 V with the P_{in} of 11.10 nW. The rise and decay time of the two samples are extracted in Figs. 4(b) and 4(c). It is found that the decay time of the two samples is similar but the rise time of the Al_2O_3 modified sample is shorter than that of the control sample. The shorter rise time could be attributed to the fact that there are fewer surface states for the Al_2O_3 modified sample. As a result, the photogenerated carrier will be transported as soon as possible without being trapped in the surface states. Further, the smaller effective mass of electrons in 2D materials caused by the tensile stress introduced by Al_2O_3 is also beneficial for improving electron mobility. It is proved that a rapid response can be achieved with the Al_2O_3 modified layer, which is suitable for improving the response time of photodetectors. Table 1 shows the comparisons of essential performance parameters of the heterojunction photodetectors in this work with some self-driven devices with similar structures. It can be seen that the performance of the detector with the Al_2O_3 layer is improved more than the control device, which proves that the Al_2O_3 layer can optimize the performance of the heterojunction detectors. The photo-responsivity of the SnS_2/WS_2 heterojunction photodetector with the Al_2O_3 layer demonstrated in this work is relatively higher than some of the reported results. Although our work has not achieved rapid response time and detectivity, it can provide a new idea for self-driven photodetectors with an oxide layer to further improve the performance.

4. Conclusion

A conductive band minimum matched self-driven SnS_2/WS_2-based van der Waals heterojunction photodetector with an Al_2O_3 capping layer has been designed and fabricated in this work. Moreover, we systematically revealed the mechanics of energy band alignment at the interface of the SnS_2/WS_2 heterostructure. However, in our previous reports, it has been proved that the Al_2O_3 stress layer can be used to improve the performance of the photodetectors. As a result, by applying the Al_2O_3 layer on the two-dimensional semiconductor materials, the performance of the self-driven photodetector has been increased. This is considered to be attributed to the Al_2O_3 modified layers introducing tensile stress, leading to a higher electron concentration and smaller effective mass of electrons in the films. The fabricated heterostructure photodetector with the Al_2O_3 modified layer shows better detection performance than that without Al_2O_3 at a 0 V bias voltage with 365 nm light radiation. Moreover, the self-driven behaviour can be attributed to the fact that there is nearly no electronic barrier in the SnS_2/WS_2 junction and the potential difference (ΔE_c) in the heterogeneous junction can be effectively adjusted by applying the bias voltage on the substrate.

Acknowledgments

Project supported by the National Natural Science Foundation of China (Grant Nos. 61974144, 62004127, and 12074263), the Science and Technology Foundation of Shenzhen (Grant No. JSGG20191129114216474), and the "National" Taipei University of Technology–Shenzhen University Joint Research Program, China (Grant No. 2020009).

References

[1] Novoselov K S, Geim A K, Morozov S V, Jiang D, Zhang Y, Dubonos S V, Grigorieva I V and Firsov A A 2004 *Science* **306** 666
[2] Novoselov K S, Jiang D, Schedin F, Booth T J, Khotkevich V V, Morozov S V, and Geim A K 2005 *Proc. Natl. Acad. Sci. USA* **102** 10451
[3] Geim A K and Novoselov K S 2007 *Nat. Mater.* **6** 183
[4] Liu X and Hersam M C 2018 *Adv. Mater.* **30** 1801586
[5] Zhang W, Wang Q, Chen Y, Wang Z and Wee A T S 2016 *2D Mater.* **3** 022001
[6] Ovchinnikov D, Allain A, Huang Y S, Dumcenco D and Kis A 2014 *ACS Nano* **8** 8174
[7] Hu Z, Wu Z, Cheng H, He J, Ni Z and Chen W 2018 *Chem. Soc. Rev.* **47** 3100
[8] Liu C, Wang B, Mu C, Zhai K, Wen F, Xiang J, Nie A and Liu Z 2020 *J. Magn. Magn. Mater.* **502** 166432
[9] Zeng L H, Wu D, Lin S H, Xie C, Yuan H Y, Lu W, Lau S P, Chai Y, Luo L B, Li Z J and Tsang Y H 2019 *Adv. Funct. Mater.* **29** 1806878
[10] Zeng L H, Chen Q M, Zhang Z X, Wu D, Yuan H Y, Li Y Y, Qarony W, Lau S P, Luo L B and Tsang Y H 2020 *Adv. Mater.* **32** 2004412
[11] Manzeli S, Ovchinnikov D, Pasquier D, Yazyev O V and Kis A 2017 *Nat. Rev. Mater.* **2** 17033
[12] Liu X K, Deng X H, Li X H, Chiu H C, Chen Y, Botcha V D, Wang M, Yu W and Lin C H 2020 *J. Alloys Compd.* **830** 154716
[13] Han J, Li J, Liu W, Li H, Fan X and Huang K 2020 *Opt. Commun.* **473** 125931
[14] Wang X, Cui Y, Li T, Lei M, Li J and Wei Z 2018 *Adv. Opt. Mater.* **7** 1801274
[15] Iqbal M W, Iqbal M Z, Khan M F, Shehzad M A, Seo Y, Park J H, Hwang C and Eom J 2015 *Sci. Rep.* **5** 10699
[16] Wei J, Wang F, Zhang B, Shan X, Di X, Li Y, Feng Y and Zhang K 2019 *Appl. Surf. Sci.* **483** 1136
[17] Ko K Y, J. Song G, Kim Y, Choi T, Shin S, Lee C W, Lee K, Koo J, Lee H, Kim J, Lee T, Park J and Kim H J 2016 *ACS Nano* **10** 9287
[18] Tian H, Chin M L, Najmaei S, Guo Q, Xia F, Wang H and Dubey M 2016 *Nano Res.* **9** 1543
[19] Wei Z M and Xia J B 2019 *Acta Phys. Sin.* **68** 163201 (in Chinese)
[20] Khan M F, Ahmed F, Rehman S, Akhtar I, Rehman M A, Shinde P A, Khan K, Kim D, Eom J, Lipsanen H and Sun Z 2020 *Nanoscale* **12** 21280
[21] Kumar S, Sharma A, Ho Y T, Pandey A, Tomar M, Kapoor A K, Chang E Y and Gupt V 2020 *J. Alloys Compd.* **835** 155222
[22] Zeng L H, Chen Q M, Zhang Z X, Wu D, Yuan H Y, Li Y Y, Qarony W, Lau S P, Luo L B and Tsang Y H 2019 *Adv. Sci.* **6** 1901134
[23] Perumal P, Ulaganathan R K, Sankar R and Zhu L 2021 *Appl. Surf. Sci.* **535** 147480
[24] Huang Y, Sutter E, Sadowski J T, Cotlet M, Monti O L A, Racke D A, Neupane M R, Wickramaratne D, Lake R K, Parkinson B A and Sutter P 2014 *ACS Nano* **8** 10743
[25] Song H S, Li S L, Gao L, Xu Y, Ueno K, Tang J, Cheng Y B and Tsukagoshi K 2013 *Nanoscale* **5** 9666
[26] Tao Y R, Wu X C, Wang W and Wang J N 2015 *J. Mater. Chem. C* **3** 1347
[27] Wu J J, Tao Y R, Wu Y and Wu X C 2016 *Sens. Actuators B* **231** 211
[28] Kuc A, Zibouche N and Heine T 2011 *Phys. Rev. B* **83** 245213
[29] Huo N, Kang J, Wei Z, Li S S, Li J and Wei S H 2014 *Adv. Funct. Mater.* **24** 7025
[30] Wang J, Xiao S, Qian W, Zhang K, Yu J, Xu X W, Wang G P, Zheng S Z and Yang S H 2021 *Adv. Mater.* **33** 2005557
[31] Liu X K, Wang J L, Xu C Y, Luo J L, Liang D S, Cen Y N, Lv Y M and Li Z W 2019 *Acta Phys.-Chim. Sin.* **35** 1134
[32] Yu J, Suleiman A A, Zheng Z, Zhou X and Zhai T 2020 *Adv. Funct. Mater.* **30** 2001650
[33] Liu X K, Chen Y X, Li D B, Wang S W, Ting C C, Chen L, Ang K A, Qiu C W, Chueh Y L, Sun X J and Kuo H C 2019 *Photonics Res.* **7** 311
[34] Wu D, Guo J W, Wang C Q, Ren X Y, Chen Y S, Lin P, Zeng L H, Shi Z F, Li X J, Shan C X and Jie J S 2021 *ACS Nano* **15** 10119
[35] Reddy C S, Willars-Rodriguez F J and Bon R R 2021 *Nanotechnology* **32** 095202
[36] Deng W J, You C Y and Zhang Y Z 2021 *IEEE Sens. J.* **21** 4044
[37] Zhou C J, Zhang S Y, Lv Z, Ma Z C, Yu C, Feng Z H and Chan M S 2020 *npj 2D Mater. Appl.* **4** 46
[38] Zhang Q L, Shou M H, Xu Y C, Zheng J X, Wen X B, Zhao Y, Wang H, Liu L L and Xie Z Q 2020 *J. Mater. Chem. C.* **8** 16506
[39] Gao W, Zhang S, Zhang F, Wen P T, Zhang L, Sun Y M, Chen H Y, Zheng Z Q, Yang M M, Luo D X, Huo N J and Li J B 2020 *Adv. Electron. Mater.* 2000964
[40] Vikraman D, Liu H, Hussain S, Karuppasamy K, Youi H K, Jung J, Kang J and Kim H S 2021 *Appl. Surf. Sci.* **543** 148863
[41] Ren X H, Wang B, Huang Z Y, Qiao H, Duan C G, Zhou Y, Zhong J X, Wang Z Y and Qi X 2021 *Flatchem* **25** 100215
[42] Li P and Zhang Z K 2020 *ACS Appl. Mater.* **12** 58132
[43] Gao S, Wang Z Q, Wang H D, Meng F X, Wang P F, Chen S, Zeng Y H, Zhao J L, Hu H G, Cao R, Xu Z Q, Guo Z N and Zhang H 2021 *Adv. Mater. Interfaces* **8** 2001730
[44] He Z B, Guo J X, Li S D, Lei Z C, Lin L, Ke Y Z, Jie W J, Gong T X, Lin Y, Cheng T D, Huang W and Zhang X S 2020 *Adv. Mater. Interfaces* **7** 1901848
[45] Wu W H, Zhang Q, Zhou X, Li L, Su J W, Wang F K and Zhai T Y 2018 *Nano Energy* **51** 45
[46] Tian H, Meng X C, Yang J H, Fan C, Yuan S, An X, Sun C, Zhang Y H, Wang M J, Zheng H X, Wei Z M and Li E P 2020 *ACS Appl. Nano Mater.* **3** 6847
[47] Whittles T J, L. Burton A, Skelton J M, Walsh A, Veal T D and Dhanak V R 2016 *Chem. Mater.* **28** 3718
[48] Wang H C, Hong Y, Chen Z, Lao C, Lu Y, Yang Z, Zhu Y and Liu X K 2020 *Nanoscale Res. Lett.* **15** 176
[49] Li K, Ang K W, Lv Y M and Liu X K 2016 *Appl. Phys. Lett.* **109** 261901
[50] Li Z, Wu J, Wang C, Zhang H, Yu W, Lu Y and Liu X 2020 *J. Nanophotonics* **9** 1579
[51] Xie Y, Wu E X, Geng G Y, Zhang D H, Hu X D and Liu J 2021 *Appl. Phys. Lett.* **118** 133103
[52] Jia C, Huang X W, Wu D, Tian Y Z, Guo J W, Zhao Z H, Shi Z F, Tian Y T, Jie J S and Li X J 2020 *Nanoscale* **12** 4435
[53] Ning J, Zhou Y, Zhang J C, Lu W, Dong J G, Yan C C, Wang D, Shen X, Feng X, Zhou H and Hao Y 2020 *Appl. Phys. Lett.* **117** 163104